Induced magnetic field stagnation point flow of nanofluid past convectively heated stretching sheet with Buoyancy effects

Tanzila Hayat and S Nadeem

Department of Mathematics, Quaid-I-Azam University 45320, *Islamabad* 44000, *Pakistan*

(Received 25 March 2016; revised manuscript received 19 May 2016; published online 30 September 2016)

This paper presents the buoyancy effects on the magneto-hydrodynamics stagnation point flow of an incompressible, viscous, and electrically conducting nanofluid over a vertically stretching sheet. The impacts of an induced magnetic field and viscous dissipation are taken into account. Both assisting and opposing flows are considered. The overseeing nonlinear partial differential equations with the associated boundary conditions are reduced to an arrangement of coupled nonlinear ordinary differential equations utilizing similarity transformations and are then illuminated analytically by using the optimal homotopy investigation strategy (OHAM). Graphs are introduced and examined for different parameters of the velocity, temperature, and concentration profile. Additionally, numerical estimations of the skin friction, local Nusselt number, and local Sherwood number are explored using numerical values.

Keywords: stretching sheet, nanofluid, boundary layer flow heat transfer

PACS: 44.20.+b, 44.05.+e, 47.15.–x **DOI:** 10.1088/1674-1056/25/11/114701

1. Introduction

A mixed convection flow is the process of heat transfer occurring as a result of the combined impacts of free convection (caused by the temperature contrast of a fluid indifferent areas) and forced convection (because of some external applied forces) flows. As of late, the investigation of mixed convection boundary layer flow past a plate has received astounding consideration as it is expected to be an essential part in various applications such as, for example, flows in the sea and in the climate, sunlight-based beneficiaries exposed to wind ebbs and flows, atomic reactors cooled in the midst of crisis shutdown, electronic gadgets cooled by fans, heat exchangers put in the short-speed atmosphere. For vertical or slanted surfaces, a solid impact can be applied by the buoyancy force.

Liquid cooling/warming is vital in different fields such as, for example, force assembling and transportation. Feasible cooling/heating methodologies are required for cooling of any sort of heat generating gadget. There are a few schedules that improve the heat transfer adequately. Some of these frameworks utilize augmented surfaces, such as the use of vibration and usage of small-scale channels to the warmth trade surfaces. By enhancing the thermal conductivity[1] of a base fluid, the capability of heat exchange can furthermore be upgraded. Subsequently, the idea of introducing particles into a normal fluid to give a superior heat transfer medium that appears as a fluid with the thermal conductivity of a metal was developed. Between each measurement of included particles (for example, full-scale, small-scale, and nanoscale), the nanosized particles have provoked additional consideration among scientists, with reference to the practicality of maintaining a consistent blend. Thermal conductivity enhancement is a special feature of nanofluids. They are imagined to delineate fluids in which nanoscaled particles are perched into the base fluids. Nanofluids are important in different modern applications including transportation, synthetic, and metallurgical parts, small-scale fabrication, power generation, and miniaturized scale fabrication. Nanofluids are used for cooling of microchips in computer and other electronic equipment that use microfluidic applications. Nanofluids, owing to their splendid joined wetting and diffusing character, are likewise vital to the generation of nanostructured material and building of complex fluids, etc. The cram of nanofluid boundary layer flow over a linearly stretched surface has received much attention in the field of several technical, industrial, and manufacturing applications (see, for instance, Refs. [2]–[4]). Crane[5] theoretically studied the boundary layer flow over a stretching surface. Subsequently, a number of characteristics of a flow with or without heat transfer stretching surface problems have been explored in many investigations (see, for instance, Refs. [6]–[9]).

Investigations of magneto-hydrodynamics (MHD) have critical applications in material science, designing, and manufacturing. Numerous metallurgical procedures include the drawing so as to cool of ceaseless strips or fibers through a motionless liquid and that during the procedure of depiction, these strips are occasionally stretched. Examples include drawing, strengthening, and furthermore, diminishing of copper wires. In all these cases, the properties of the final product depend, as it were, on the rate of cooling by sketching such strips in an electrically conducting fluid along with the magnetic field and the desired quality of the final product. Mahapatra and Gupta[10] numerically examined the heat transfer stagnation point flow over a stretching sheet with a magnetic field. Makinde[11] reported the similarity solution by stagna-

© 2016 Chinese Physical Society and IOP Publishing Ltd

tion point MHD mixed convection flow toward a vertical plate fixed in a highly porous standard with internal heat generation and radiation. Nanofluids attract much interest in light of their gigantic potential to give improved execution properties, especially concerning heat exchange. Since the pioneering work of Choi,[12] studies related to the nanofluid dynamics have increased greatly in recent times because of its extensive applications in industrial and manufacturing systems.[13] A complete audit of the research on nanofluids is given by Refs. [14]–[16]. The stagnation point flow of a nanofluid towards a stretching sheet was investigated by Mustafa *et al.*[17] Khan and Pop[18] analyzed nanofluid boundary layer flow past a stretching sheet. Later on, Khan and Aziz[19] utilized the similar replica to explore the nanofluid boundary layer flow past a vertical surface along with a steady warmth flux. Recently, Ibrahim *et al.*[20] numerically investigated the hydro magnetic stagnation point heat transfer flow of a nanofluid towards a stretching sheet. Their outcomes demonstrate that the rate of heat exchange at the sheet surface increases with the magnetic parameter when the free stream speed surpasses the stretching speed. The boundary layer against a vertical surface issue was analyzed by Ishak *et al.*[21,22] However, in micropolar fluid, Lok *et al.*[23] and Ishak *et al.*[24] studied the stagnation point boundary layer flow on a vertical surface. Zhang *et al.*[25–29] studied the MHD radiation heat transfer flow of nanofluids for both steady and unsteady cases over a stretching surface.

These are studies where the induced magnetic fields are not considered.The investigation of magnetic field boundary layer flow with the induced magnetic field has been considered by certain researchers. For example, Raptis and Perdikis,[30] Kumari *et al.*,[31] and Takhar *et al.*[32] studied a free convection flow. Ali *et al.*[33] considered MHD mixed convection boundary layer flow with induced magnetic field. Ali *et al.*[34] studied the thermal reversal stagnation point flow with induced magnetic field. Regardless of several works that have been reported on flow and heat transfer of nanofluids, there seem to be no attempts in literature to consider the combined effects of buoyancy force and convective heating on MHD stagnation point flow and heat transfer of nanofluid towards a stretching surface with induced magnetic field.

Inspired by the above analysis, our objective is to analyze the combined effects of buoyancy force convective heating, Brownian, and thermophoresis motion on MHD stagnation point flow and heat transfer of electrically conducting nanofluid towards a stretching sheet under the influence of induced magnetic field. The obtained nonlinear partial differential equations are solved analytically by using the optimal homotopy analysis method (OHAM).[35–40] After employing OHAM, the obtained nonlinear equations are solved analytically. The results are discussed by considering graphical and tabulated forms.

2. Mathematical formulation

Let us suppose the steady two-dimensional stagnation point flow of an incompressible electrically conducting nanofluid over a stretching sheet at $y = 0$. The flow occupies the domain $y > 0$. The sheet is stretched along the x axis with a velocity ax, where $a > 0$ is the stretching parameter. The fluid velocity and nanoparticles concentration near the surface are assumed to be $U_{\rm w}$ and $C_{\rm w}$, respectively. The ambient fluid temperature and concentration are taken as T_∞ and C_∞, while the temperature of the surface is maintained by convective heat transfer at a certain value $T_{\rm f}$. The impact of the induced magnetic field is additionally considered as shown in Fig. 1. The general transport equations for the nanofluid along with the induced magnetic field can be written as

$$\boldsymbol{\nabla}\cdot\boldsymbol{V}=0, \tag{1}$$

$$\boldsymbol{\nabla}\cdot\boldsymbol{H}=0, \tag{2}$$

$$\begin{aligned}&(\boldsymbol{V}\cdot\boldsymbol{\nabla})\boldsymbol{V}-\frac{\mu_{\rm f}}{4\pi\rho}(\boldsymbol{H}\cdot\boldsymbol{\nabla})\boldsymbol{H}\\ &=\frac{1}{\rho}\boldsymbol{\nabla}\cdot\boldsymbol{S}\pm\frac{1}{\rho_{\rm f}}[(1-C_\infty)\rho_{\rm f\infty}\beta_0 g(T-T_\infty)\\ &\quad-(\rho_{\rm p}-\rho_\infty)g(C-C_\infty)],\end{aligned} \tag{3}$$

$$\boldsymbol{\nabla}\times(\boldsymbol{V}\times\boldsymbol{H})+\alpha_1\boldsymbol{\nabla}^2\boldsymbol{H}=0, \tag{4}$$

$$\begin{aligned}&\rho_{\rm f}c_{\rm f}\frac{{\rm d}T}{{\rm d}t}\\ &=\boldsymbol{\nabla}\cdot k\boldsymbol{\nabla}T+\mu_{\rm f}(\nabla\boldsymbol{V})^2\\ &\quad+\rho_{\rm p}c_{\rm p}\left(D_{\rm B}\boldsymbol{\nabla}\phi\cdot\boldsymbol{\nabla}T+D_{\rm T}\frac{\nabla T\cdot\nabla T}{T_\infty}\right),\end{aligned} \tag{5}$$

$$\boldsymbol{V}\cdot\boldsymbol{\nabla}C=\boldsymbol{\nabla}\cdot\left(D_{\rm B}\boldsymbol{\nabla}C+D_{\rm T}\frac{\boldsymbol{\nabla}T}{T_\infty}\right), \tag{6}$$

where $\boldsymbol{V}(u(x,y),v(x,y),0)$ and $\boldsymbol{H}(H_1(x,y),H_2(x,y),0)$ are the velocity and induced magnetic field vectors respectively, $\rho_{\rm f}$ is the nanofluid density, $\boldsymbol{S}$ is the Cauchy stress tensor, $\rho_{\rm f}c_{\rm f}$ and $\rho_{\rm p}c_{\rm p}$ are nanofluid and nanoparticle heat capacities, respectively, T is temperature, k is the nanofluid thermal conductivity, $D_{\rm B}$ is the Brownian diffusion coefficient, C is the nanoparticle volumetric fraction, $D_{\rm T}$ is the thermophoretic diffusion coefficient, g is the gravity acceleration, μ, ν, σ, and $\alpha_1 = 1/4\pi\sigma$ represent the magnetic permeability, kinematic viscosity, electrical conductivity, and magnetic diffusivity, respectively. In addition, the MHD pressure is given by

$$P=p+\frac{\mu|\boldsymbol{H}|^2}{8\pi}, \tag{7}$$

where p is the pressure of the fluid.

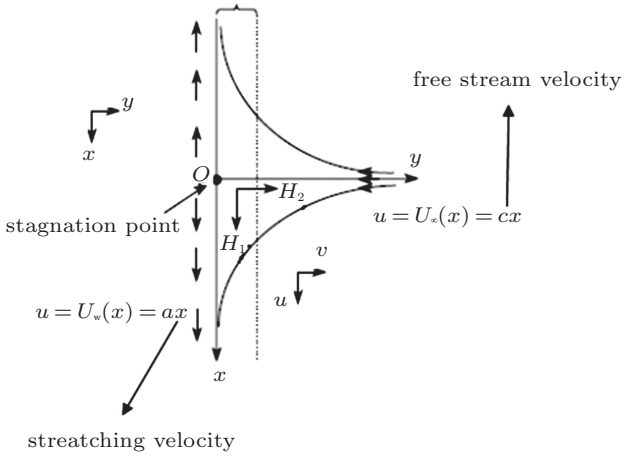


Fig. 1. Schematic plot of the problem.

Under the Boussinesq and boundary layer approximation, basic equations can be written as

$$\frac{\partial u}{\partial x}+\frac{\partial v}{\partial y}=0, \tag{8}$$

$$\frac{\partial H_1}{\partial x}+\frac{\partial H_2}{\partial y}=0, \tag{9}$$

$$\begin{aligned} &u\frac{\partial u}{\partial x}+v\frac{\partial u}{\partial y}\\ &=U_\infty\frac{\mathrm{d}U_\infty}{\mathrm{d}x}+\nu\frac{\partial^2 u}{\partial y^2}-\frac{\mu_\mathrm{f}}{4\pi\rho}\left(H_\infty\frac{\mathrm{d}H_\infty}{\mathrm{d}x}\right)\\ &+\frac{\mu_\mathrm{f}}{4\pi\rho}\left(H_1\frac{\partial H_1}{\partial x}+H_2\frac{\partial H_2}{\partial y}\right)\\ &\pm\frac{1}{\rho_\mathrm{f}}[(1-C_\infty)\rho_{\mathrm{f}\infty}\beta_0 g(T-T_\infty)\\ &-(\rho_\mathrm{p}-\rho_\infty)g(C-C_\infty)], \end{aligned} \tag{10}$$

$$u\frac{\partial H_1}{\partial x}+v\frac{\partial H_1}{\partial y}-H_1\frac{\partial u}{\partial x}-H_2\frac{\partial u}{\partial y}=\alpha_1\frac{\partial^2 H_1}{\partial y^2}, \tag{11}$$

$$\begin{aligned} &u\frac{\partial T}{\partial x}+v\frac{\partial T}{\partial y}\\ &=\alpha_\mathrm{f}\frac{\partial^2 T}{\partial y^2}+\frac{\mu\alpha_\mathrm{f}}{k}\left(\frac{\partial u}{\partial y}\right)^2\\ &+\tau\left(D_\mathrm{B}\frac{\partial C}{\partial y}\frac{\partial T}{\partial y}+\frac{D_\mathrm{T}}{T_\infty}\left(\frac{\partial T}{\partial y}\right)^2\right), \end{aligned} \tag{12}$$

$$u\frac{\partial C}{\partial x}+v\frac{\partial C}{\partial y}=D_\mathrm{B}\frac{\partial^2 C}{\partial y^2}+\frac{D_\mathrm{T}}{T_\infty}\frac{\partial^2 T}{\partial y^2}, \tag{13}$$

where α_f is the thermal diffusivity of the nanofluid and $\tau=\rho_\mathrm{p}c_\mathrm{p}/\rho_\mathrm{f}c_\mathrm{f}$ is the ratio of heat capacity of the nanoparticle to the base fluid. The corresponding boundary conditions are

$$\begin{aligned} &u=U_\mathrm{w}=ax,\ v=0,\ \frac{\partial H_1}{\partial y}=H_2=0,\ -k\frac{\partial T}{\partial y}=h_\mathrm{f}(T_\mathrm{f}-T),\\ &C=C_\mathrm{w}\text{ at }y=0,\ u=U_\infty=cx, H_1=H_\infty=H_0x,\\ &T=T_\infty, C=C_\infty\text{ as }y\to\infty. \end{aligned} \tag{14}$$

Here, H_0 is an estimation of the uniform magnetic field at the upstream infinity and c and a are the positive constants determining the strength of the stagnation point and stretching rate of the sheet, respectively. Introducing the following transformations:

$$\begin{aligned} &\eta=\sqrt{\frac{a}{\nu}}y,\ u=axf'(\eta),\ v=-\sqrt{a\nu}f(\eta),\ \theta=\frac{T-T_\infty}{T_\mathrm{f}-T_\infty},\\ &\phi=\frac{C-C_\infty}{C_\mathrm{w}-C_\infty},\ H_1=H_0xg'(\eta),\ H_2=-H_0\sqrt{\frac{\nu}{a}}g(\eta). \end{aligned} \tag{15}$$

With the help of the above transformations, equations (8) and (9) are identically satisfied and equations (10)–(13) along with boundary conditions (14) are given by

$$\begin{aligned} &f'''+ff''-f'^2+\lambda^2+\beta(g'^2-gg''-1)\\ &\pm Q(\theta-Nr\phi)=0, \end{aligned} \tag{16}$$

$$\varepsilon g'''+fg''-gf''=0, \tag{17}$$

$$\theta''+\mathrm{Pr}(f\theta'+N_\mathrm{b}\phi'\theta'+N_\mathrm{t}\theta'^2+\mathrm{Ec}f''^2)=0, \tag{18}$$

$$\phi''+\frac{N_\mathrm{t}}{N_\mathrm{b}}\theta''+(\mathrm{PrLe})f\phi'=0, \tag{19}$$

$$\begin{aligned} &f=0,\ f'=1,\ g=0,\ g''=0,\ \theta'=-\mathrm{Nc}[1-\theta],\\ &\phi=1\text{ at }\eta=0,\\ &f'=\lambda,\ g'=1,\ \theta=0,\ \phi=0\text{ as }\eta\to\infty, \end{aligned} \tag{20}$$

where f, g, θ, and ϕ are functions of η and the prime represent derivative with respect to η, ε is the inverse of magnetic Prandtl number, β is the magnetic parameter, and λ, Nr, Q, Nc, Pr, Ec, N_b, N_t, and Le are the stretching parameter, buoyancy ratio, gravity-dependent parameter, convective parameter, Prandtl number, Ecket number, nanofluid parameters, and Lewis number, respectively. Additionally, β_0 is the volumetric thermal expansion coefficient which is defined as

$$\begin{aligned} &\lambda=\frac{c}{a},\ \mathrm{Nr}=\frac{(\rho_\mathrm{p}-\rho_\infty)(C_\mathrm{w}-C_\infty)}{\rho\beta_0(1-C_\infty)(T_\mathrm{f}-T_\infty)},\\ &Q=\pm r=\frac{(1-C_\infty)(T_\mathrm{f}-T_\infty)\beta_0 g}{a^2x},\\ &\varepsilon=\frac{\alpha_1}{\upsilon},\ \beta=\frac{\mu_\mathrm{f}}{L^2\rho}\left(\frac{H_0}{a}\right)^2,\ \mathrm{Pr}=\frac{\upsilon}{\alpha},\ \mathrm{Nc}=\sqrt{\frac{\upsilon}{a}}\frac{h_\mathrm{f}}{k},\\ &\mathrm{Ec}=\frac{a^2x^2\rho\alpha_\mathrm{f}}{k(T_\mathrm{f}-T_\infty)},\ N_\mathrm{b}=\frac{\tau D_\mathrm{B}(C_\mathrm{w}-C_\infty)}{\upsilon},\\ &N_\mathrm{t}=\frac{\tau D_\mathrm{T}(T_\mathrm{f}-T_\infty)}{\upsilon T_\infty},\ \mathrm{Le}=\frac{\alpha_\mathrm{f}}{D_\mathrm{B}}. \end{aligned}$$

Here, $N_\mathrm{b}=0$ compares to the situation when there is no thermal transport produced by nanoparticle concentration gradients. When Nc = ∞, the convective boundary condition decreases to a uniform surface temperature boundary condition. The physical factors of interest are the local skin friction coefficient c_f, local Nusselt number Nu, and local Sherwood number Sh, which are defined as

$$\begin{aligned} &c_\mathrm{f}=\frac{\tau_\mathrm{w}}{\rho U_\mathrm{w}^2},\ \mathrm{Nu}=\frac{-x}{T_\mathrm{f}-T_\infty}\frac{\partial T}{\partial y}\bigg|_{y=0},\\ &\mathrm{Sh}=\frac{-x}{C_\mathrm{w}-C_\infty}\frac{\partial C}{\partial y}\bigg|_{y=0}, \end{aligned} \tag{21}$$

or by introducing the transformations (15), we have

$$\sqrt{\mathrm{Re}}c_{\mathrm{f}} = [f''^{2}]_{\eta=0},\ \frac{\mathrm{Nu}}{\sqrt{\mathrm{Re}}} = -\theta'(0),\ \frac{\mathrm{Sh}}{\sqrt{\mathrm{Re}}} = -\phi'(0). \quad (22)$$

Here, $\mathrm{Re} = ax^2/\nu$ is a local Reynolds number. The physical parameters will be discussed later in the outcomes segment.

3. Solution technique

Nonlinearity plays a vital role in physical phenomena. Liao[26] proposed a method to solve nonlinear problems that is known as the optimal homotopy analysis method (OHAM). To be more explicit, the governing equations are nonlinear even in viscous fluids. The most general method that is extensively used by scholars is the perturbation method. In the problem statement, this method requires large/small parameters. Lately some other methods such as homotopy analysis, Adomian, homotopy perturbation, etc., have become more attractive by the researchers in various fields. The optimal homotopy analysis method (OHAM) is preferred among all these because of the following reasons:

(i) OHAM does not necessitate any large/small parameter in the problem.

(ii) The convergence region can be controlled easily.

(iii) The rate of approximations series is modifiable.

(iv) It delivers freedom to choose altered sets of base functions. The initial guesses and operators are taken as

$$\begin{aligned} f_0(\eta) &= \lambda\eta + (1-\lambda)(1-\exp(-\eta)),\\ g_0(\eta) &= \eta,\\ \theta_0(\eta) &= \left(\frac{\mathrm{Nc}}{1+\mathrm{Nc}}\right)\exp(-\eta),\\ \phi_0(\eta) &= \exp(-\eta), \end{aligned} \quad (23)$$

$$\begin{aligned} L_{\mathrm{f}}(f) &= \frac{\mathrm{d}^3 f}{\mathrm{d}\eta^3} - \frac{\mathrm{d}f}{\mathrm{d}\eta},\\ L_g(g) &= \frac{\mathrm{d}^3 g}{\mathrm{d}\eta^3} - \frac{\mathrm{d}g}{\mathrm{d}\eta},\\ L_\theta(\theta) &= \frac{\mathrm{d}^2\theta}{\mathrm{d}\eta^2} + \frac{\mathrm{d}\theta}{\mathrm{d}\eta},\\ L_\phi(\phi) &= \frac{\mathrm{d}^2\phi}{\mathrm{d}\eta^2} + \frac{\mathrm{d}\phi}{\mathrm{d}\eta}. \end{aligned} \quad (24)$$

Table 1. Convergence of parametric values for average residual ($\varepsilon_{\mathrm{m}}^{\mathrm{t}}$) are shown below by optimal analysis method (OHAM).

	h_{f}	h_{g}	h_θ	h_ϕ	$\varepsilon_{\mathrm{m}}^{\mathrm{t}}$
2	−1.12971	−1.48394	−0.91200	−1.04128	0.00327789
4	−1.568361	−1.32509	−1.1456	−1.24352	0.000831667
6	−1.57064	−1.30341	−1.16717	−1.36853	0.000262031
8	−1.57809	−1.31557	−1.1836	−1.43935	9.32448×10^{-5}

Table 2. Individual residual square errors for $\varepsilon_{\mathrm{m}}^{\mathrm{f}}$, $\varepsilon_{\mathrm{m}}^{\mathrm{g}}$, $\varepsilon_{\mathrm{m}}^{\theta}$, and $\varepsilon_{\mathrm{m}}^{\phi}$.

	$h_{\mathrm{f}} = -1.57809$	$h_{\mathrm{g}} = -1.31557$	$h_\theta = -1.1836$	$h_\phi = -1.43935$
	$\varepsilon_{\mathrm{m}}^{\mathrm{f}}$	$\varepsilon_{\mathrm{m}}^{\mathrm{g}}$	$\varepsilon_{\mathrm{m}}^{\theta}$	$\varepsilon_{\mathrm{m}}^{\phi}$
4	4.17243×10^{-6}	9.07369×10^{-6}	0.000145677	0.00200841
8	8.4256×10^{-8}	1.69239×10^{-6}	0.0000137039	0.0000777642
12	7.67956×10^{-8}	3.73585×10^{-7}	5.6952×10^{-6}	0.0000191108
18	2.60796×10^{-8}	7.12435×10^{-8}	1.75073×10^{-6}	7.97497×10^{-6}

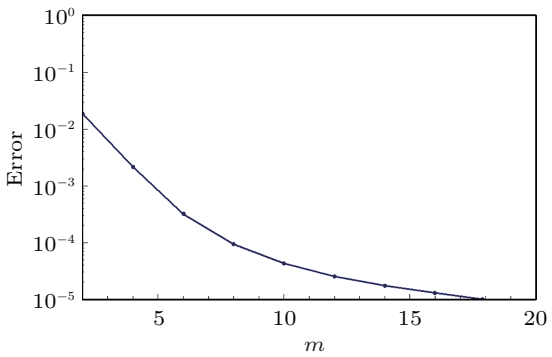


Fig. 2. Graphical representation for 8th order approximation.

4. Graphical results and discussion

In this section, the primary focus of this article is to examine the attributes of stagnation-point flow of a viscous incompressible nanofluid over a stretching sheet in the region of an induced magnetic field with convective boundary conditions. For this reason, the computations have been performed by using optimal homotopy analysis method for various estimations of the parameters. In addition, the accuracy of the present results is affirmed by comparing them and the already recorded results. Presently, we give the graphical elucidation of our outcomes. Figures 3 and 4 show the effects of the buoyancy-ratio Nr on the velocity profile. It can be clearly seen that the velocity profile f' increases as the buoyancy ratio Nr increases for the case of opposing flow while the opposite behavior is observed for assisting flow. This is because for opposing flow Nr acts as a supportive driving force that accelerates the motion of

the fluid. This is why the velocity profile increases in Fig. 3. From Fig. 5, the magnetic parameter β shows the effects on the g' profile. It is seen that the velocity g' profile increases when the magnetic parameter β increases. Figures 6 and 7 show the effects of the magnetic parameter β on velocity g' profile. It is seen that the g' profile decreases by increasing the magnetic parameter β (when $\lambda \geq 1$). Physically, when $\lambda < 1$, the stretching velocity ax of the surface exceeds the velocity cx of the free stream while the opposite behavior is observed when $\lambda \geq 1$, i.e., the boundary layer thickness decreases as λ increases for the case of $\lambda \geq 1$. It can likewise be clarified with respect to the fixed estimation of a, the increment in c in correlation to a suggests the increase in the straining movement close to the stagnation area that can increase the acceleration of the free stream. Therefore, by increasing λ, the boundary layer thickness decreases. Figure 8 shows the effects of the stretching parameter λ on the g' profile. We notice that the g' profile decreases by increasing λ. From Figs. 9 and 10, it is found that in the absence and presence of the magnetic parameter β for both opposing and assisting flows, the thermal boundary layer thickness decreases as λ increases. Figure 11 shows the effects of the Prandtl number Pr on the temperature field. The thermal diffusivity will decrease if the Prandtl number Pr increases. Thus, as an outcome, the energy transfer capacity decreases and the thermal boundary layer also decreases. On the off chance that Pr increases, the thermal diffusivity will diminish. This prompts the diminishing of the energy exchange capacity, and results in the lessening thermal boundary layer. From Figs. 12 and 13, again both $\beta = 0$ and $\beta = 0.2$ are considered for opposing and assisting flow. It is found that both the concentration profile and the concentration boundary layer thickness decrease as λ increases. The behavior of the Lewis number Le on the concentration profile is presented in Fig. 14. As Le gradually increases, this corresponds to a weaker molecular diffusivity and thinner concentration boundary layer. To verify the legitimacy and accuracy of the obtained numerical results, the estimations of the skin friction coefficient $f''(0)$ without magnetic field are contrasted with previously published results as shown in Table 3. They demonstrate great understanding. The values of the skin friction coefficient $f''(0)$ are shown in Table 4. It shows variations of $C_f \mathrm{Re}^{1/2}$ for different λ, ε, Ec, Nr, and r. As shown, when the stretching parameter λ and the buoyancy ratio Nr increase, $f''(0)$ decreases. When the reciprocal of the magnetic Prandtl number ε and Eckert number Ec increases, $f''(0)$ increases. $f''(0)$ increases by increasing positive gravity-dependent parameter while the opposite behavior is observed when $r < 0$. Table 5 shows the variations of $\mathrm{NuRe}^{1/2}$ for different λ, ε, Ec, Pr, and r. When the stretching parameter λ and Prandtl number Pr increase, $\mathrm{Nu}_x\mathrm{Re}^{-1/2}$ increases. When Eckert number Ec increases, $\mathrm{Nu}_x\mathrm{Re}^{-1/2}$ decreases. That is, heat has begun spilling out of the liquid to the surface. Therefore, we draw imperative result that the viscous dissipation may bring about an adjustment toward heat exchange. In this way, the viscous dissipation ought to be thought about while examining the stagnation point boundary layer flows. By increasing the reciprocal of magnetic Prandtl number ε, $\mathrm{Nu}_x\mathrm{Re}^{-1/2}$ remains constant. Table 6 shows the variations of $\mathrm{Sh}_x\mathrm{Re}^{-1/2}$ for different λ, ε, Nr, N_b, and N_t. Here we see that, when the stretching parameter λ, nanofluid parameter N_b, and the reciprocal of the magnetic Prandtl number λ increases, $\mathrm{Sh}_x\mathrm{Re}^{-1/2}$ also increases. By increasing buoyancy ratio Nr and nanofluid parameter N_t, $\mathrm{Sh}_x\mathrm{Re}^{-1/2}$ decreases. Table 7 shows the effect of induced magnetic field on C_f, Nu_x, and Sh_x. We observed that by increasing the magnetic parameter β, C_f, Nu_x, and Sh_x decreases while by increasing the reciprocal of the magnetic Prandtl number ε, C_f increases but Nu_x, and Sh_x both decrease.

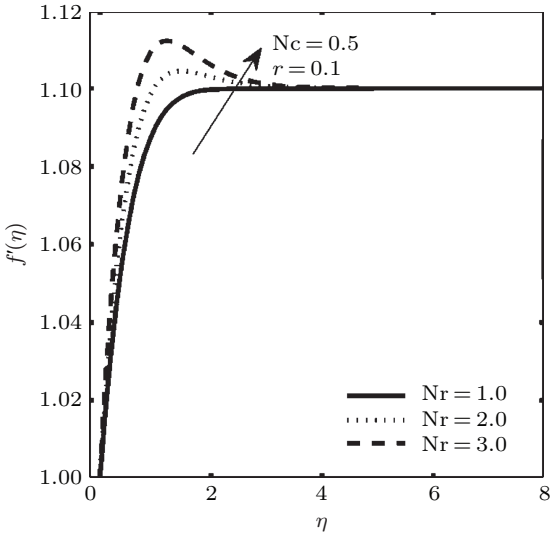


Fig. 3. Variation of $f'(\eta)$ for different values of buoyancy-ratio Nr with β = 0.15, λ = 1.1, Pr = 1, $N_b = N_t$ = Ec = 0.1, ε = 1.5, and Le = 1.

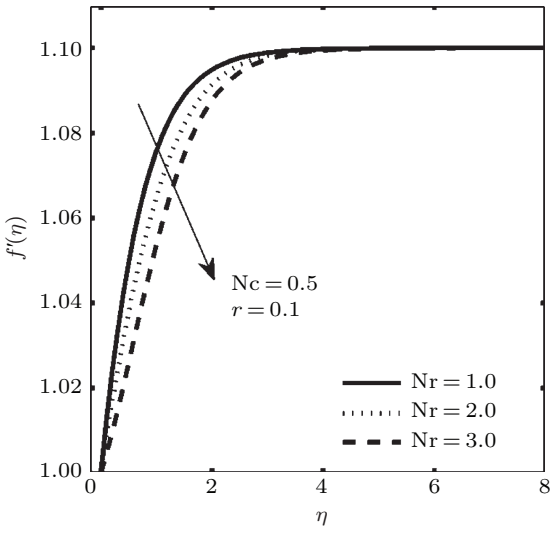


Fig. 4. Variation of $f'(\eta)$ for different values of buoyancy ratio Nr with β = 0.15, λ = 1.1, Pr = 1, $N_b = N_t$ = Ec = 0.1, ε = 1.5, and Le = 1.

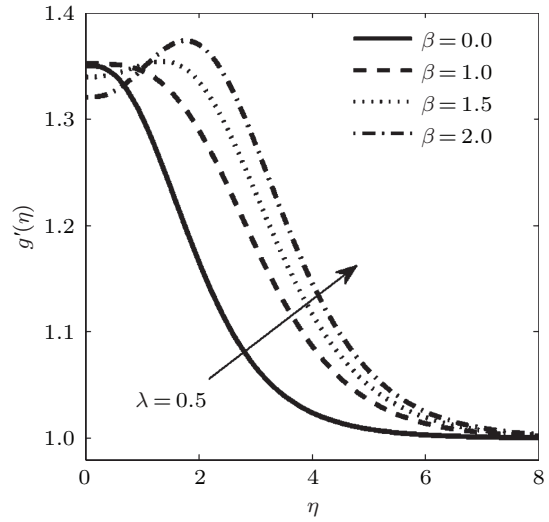


Fig. 5. Variation of $g'(\eta)$ for different values of magnetic parameter β with Nc = 0.5, Pr = 1, $N_b = N_t$ = Nr = r = Ec = 0.1, ε = 1.5, and Le = 1.

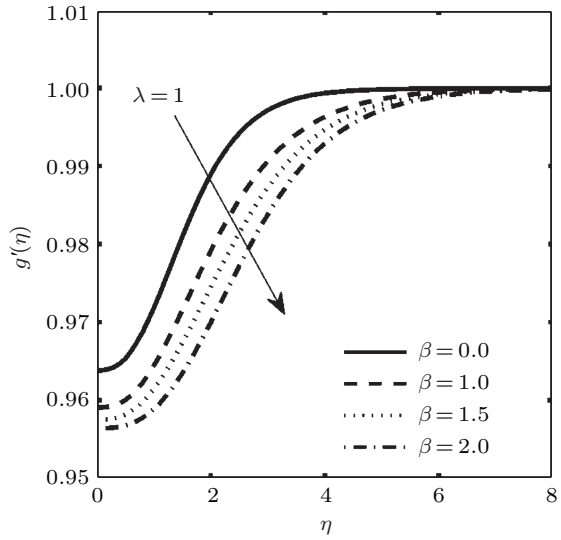


Fig. 6. Variation of $g'(\eta)$ for different values of magnetic parameter β with Nc = 0.5, Pr = 1, $N_b = N_t$ = Nr = r = Ec = 0.1, ε = 1.5, and Le = 1.

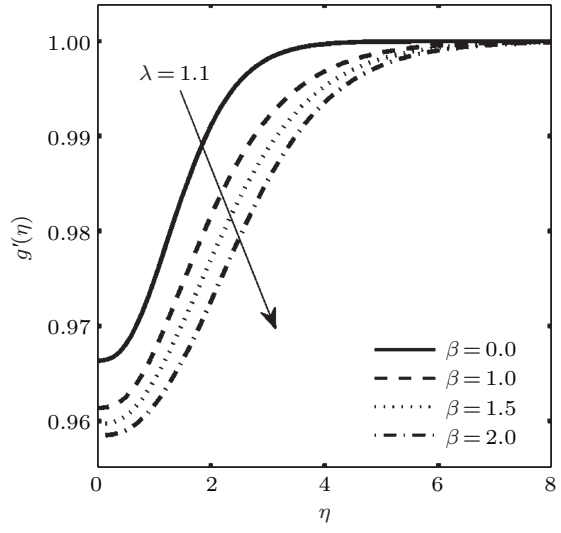


Fig. 7. Variation of $g'(\eta)$ for different values of magnetic parameter β with Nc = 0.5, Pr = 1, $N_b = N_t$ = Nr = r = Ec = 0.1, ε = 1.5, and Le = 1.

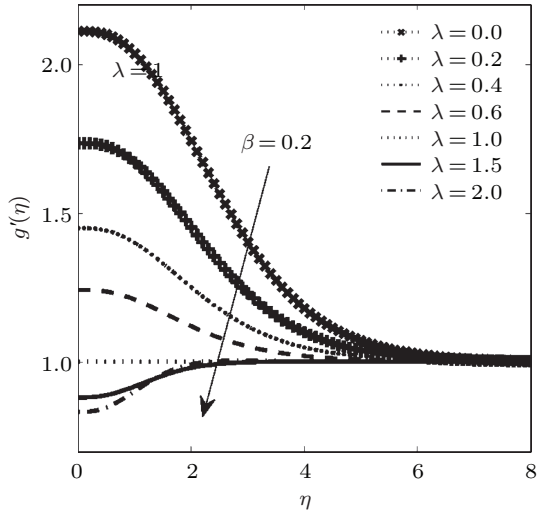


Fig. 8. Variation of $g'(\eta)$ for different values of magnetic parameter β with Nc = 0.5, Pr = 1, $N_b = N_t$ = Nr = r = Ec = 0.1, ε = 1.5, and Le = 1.

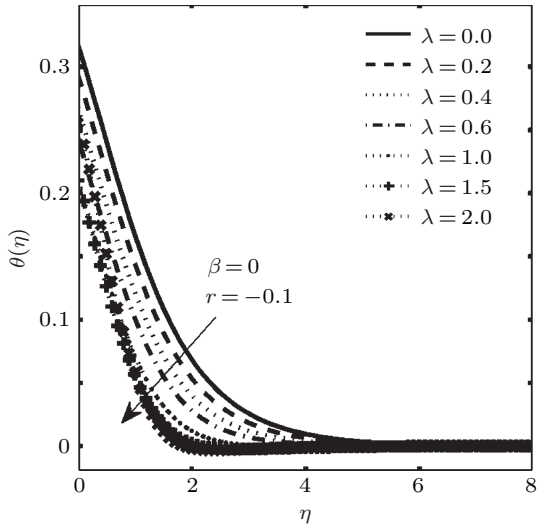


Fig. 9. Variation of $\theta(\eta)$ for different values of stretching parameter λ with Nc = 0.2, Pr = 1, $N_b = N_t$ = Nr = r = Ec = 0.1, ε = 1.5, and Le = 1.

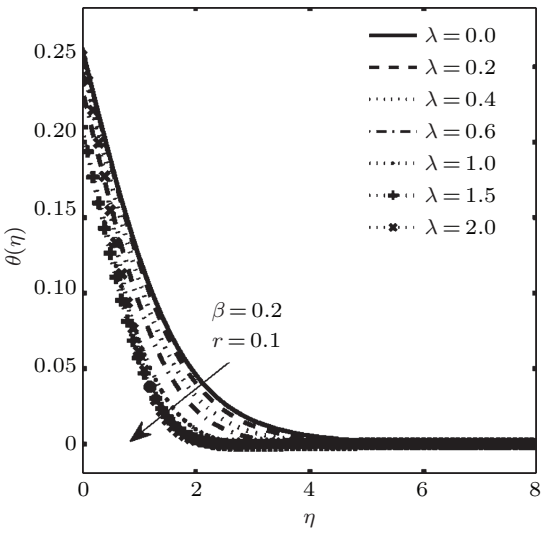


Fig. 10. Variation of $\theta(\eta)$ for different values of stretching parameter λ with Nc = 0.2, Pr = 1, $N_b = N_t$ = Nr = r = Ec = 0.1, ε = 1.5, and Le = 1.

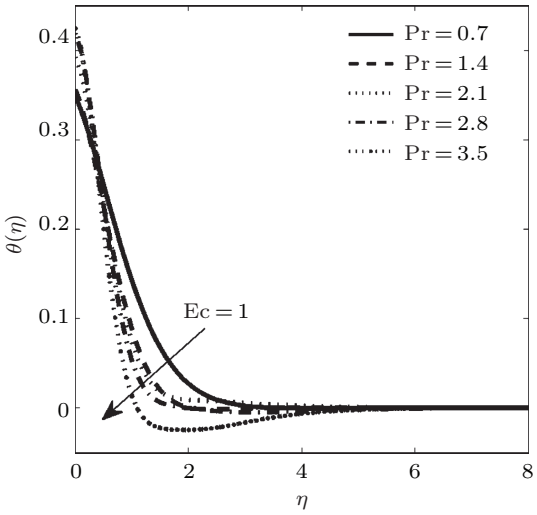


Fig. 11. Variation of $\theta(\eta)$ for different values of Prandtl number Pr with Nc = 0.2, λ = 1.5, β = 0.75, $N_b = N_t$ = Nr = r = 0.1, ε = 1, and Le = 1.

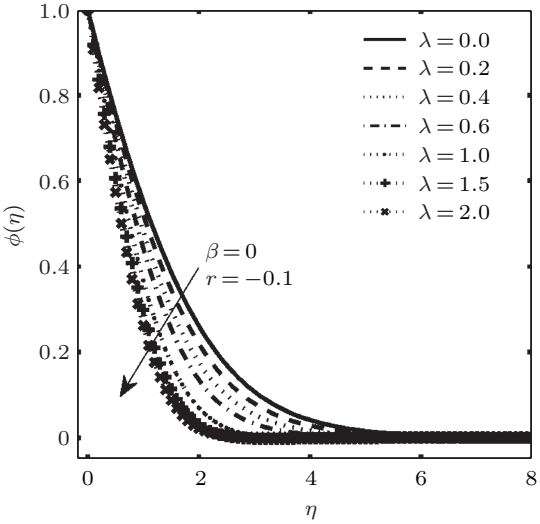


Fig. 12. Variation of $\phi(\eta)$ for different values of stretching parameter λ with Nc = 0.2, Pr = 1, $N_b = N_t$ = Nr = r = Ec = 0.1, ε = 1.5, Le = 1 are fixed.

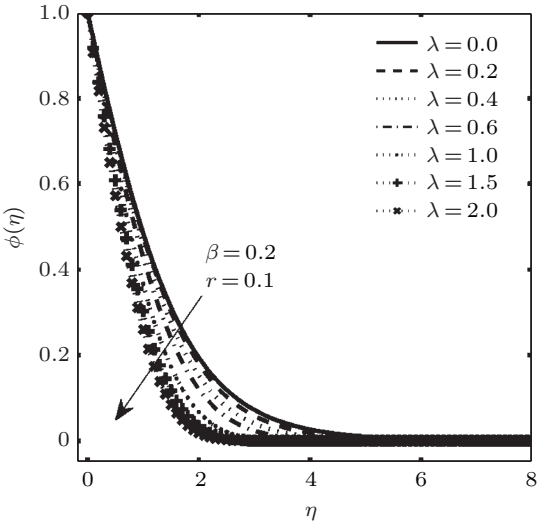


Fig. 13. Variation of $\phi(\eta)$ for different values of stretching parameter λ with Nc = 0.2, Pr = 1, $N_b = N_t$ = Nr = r = Ec = 0.1, ε = 1.5, and Le = 1.

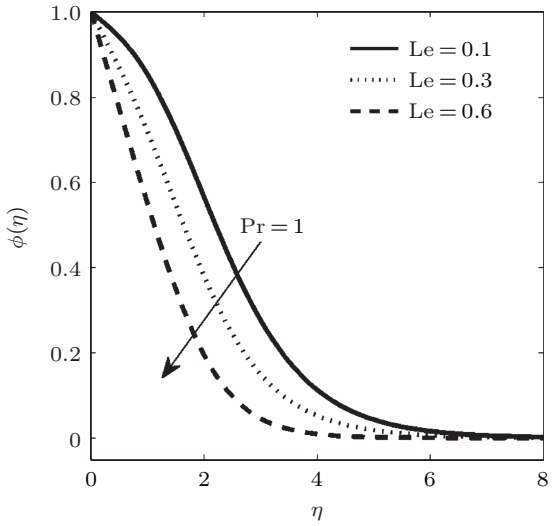


Fig. 14. Variation of $\phi(\eta)$ for different values of Lewis number Le with Nc = 0.5, λ = 1.1, $N_b = N_t$ = Nr = r = Ec = 0.1, ε = 1.5, and β = 0.15.

Table 3. Skin friction coefficient C_f with different values of λ in the absence of magnetic field, i.e., $\beta = 0$.

λ	Mahapatra and Gupta	Nazar *et al.*	Ishak *et al.*	Present result
0.1	−0.9694	−0.9694	−0.9694	−0.9694
0.5	−0.6673	−0.6673	−0.6673	−0.6672
3	4.7293	4.7296	4.7294	4.7295

Table 4. Variation of skin friction C_f with different parameters.

λ	ε	Ec	Nr	R	$C_f \mathrm{Re}^{1/2}$
0.0	1.5	0.1	0.1	0.1	−0.995493
0.1					−0.898426
0.5					−0.501592
1.1	1.0	0.1	0.1	0.1	0.101078
	1.5				0.101331
	2.0				0.101989
1.1	1.5	0.1	0.1	0.1	0.101331
		0.5			0.102206
		1.0			0.102368
1.1	1.5	0.1	0.1	0.1	0.101331
			0.5		0.100606
			1.0		0.100274
1.1	1.5	0.1	0.1	0.0	0.100860
				0.1	0.101091
				0.3	0.101899
				-0.1	0.100791
				−0.3	0.100707

Table 5. Variation of Nusselt number Nu with different parameters.

λ	ε	Ec	Pr	R	$\mathrm{Nu}_x\mathrm{Re}^{-1/2}$
0.0	1.5	0.1	0.1	1	0.135953
0.1					0.140165
0.5					0.151500
1.1	1.0	0.1	1	0.1	0.158621
	1.5				0.158621
	2.0				0.158621
1.1	1.5	0.1	1	0.1	0.158648
		0.5			0.158292
		1.0			0.157892
1.1	1.5	0.1	0.72	0.1	0.153161
			1.0		0.158648
			1.3		0.162302
1.1	1.5	0.1	1	0.0	0.158490
				0.1	0.158592
				0.3	0.158647
				−0.1	0.158490
				−0.3	0.158550

Table 6. Variation of Sherwood number Sh with different parameters.

λ	ε	Nr	N_b	N_t	$\mathrm{Sh}_x\mathrm{Re}^{-1/2}$
0.0	1.5	0.1	0.1	0.1	0.585354
0.1					0.592144
0.5					0.632763
1.1	1.0	0.1	0.1	0.1	0.742869
	1.5				0.743078
	2.0				0.743134
1.1	1.5	0.1	0.1	0.1	0.744216
		0.5			0.743053
		1.0			0.741505
1.1	1.5	0.1	0.1	0.1	0.744216
			0.5		0.806788
			1.0		0.816729
1.1	1.5	0.1	0.1	0.1	0.744216
				0.5	0.457038
				1.0	0.124515

Table 7. Effect of induced magnetic field on C_f, Nu_x, and Sh_x when Nc = 0.2, Ec = r = Nr = N_b = N_t = 0.1, λ = 1.1, Le = 1, and Pr = 1.

β	ε	$C_\mathrm{f}\mathrm{Re}^{1/2}$	$\mathrm{Nu}_x\mathrm{Re}^{-1/2}$	$\mathrm{Sh}_x\mathrm{Re}^{-1/2}$
0	1.5	0.168376	0.158817	0.744361
0.2		0.159333	0.158795	0.743906
0.5		0.143776	0.158730	0.741125
0.15	1	0.101078	0.158801	0.743640
	1.5	0.101331	0.158748	0.743078
	2	0.101989	0.158709	0.743044

5. Concluding remarks

We have discussed the MHD stagnation-point flow of a viscous incompressible nanofluid over a stretching sheet in the vicinity of an induced magnetic field. In this study, we observe that there are noteworthy impacts of the magnetic parameter on the velocity, g, temperature, and concentration profiles. We can conclude that

(i) By increasing the buoyancy ratio Nr for opposing flow, the velocity profile f' increases; however, it demonstrates the opposite conduct for assisting flow.

(ii) By increasing magnetic parameter β, g' increases when $\lambda < 1$, while it decreases for $\lambda \geq 1$.

(iii) As the magnetic parameter β increases, C_f, Nu_x, and Sh_x decrease.

(iv) By increasing the stretching parameter λ and Prandtl number Pr, g' decreases.

(v) In the absence of the magnetic parameter β together with assisting opposing flow, the temperature profile decreases.

(vi) In the presence of the magnetic parameter β for assisting flow, the temperature profile decreases.

(vii) By increasing the Prandtl number Pr, the temperature profile decreases.

(viii) In the absence and presence of the magnetic parameter β with gravity-dependent parameter for both cases ($r < 0$, $r > 0$), the concentration profile φ decreases by increasing the stretching parameter λ.

(v) The concentration profile φ decreases by increasing Lewis number Le.

References

[1] Choi U S 1995 *ASME FED* **231** 99
[2] Azmi W H, Hamid Abdul K, Usri N A, Mamat Razilman and Sharma K V 2016 *Int. Comm. Heat Mass Trans.* **75** 13
[3] Li X K, Zou C J, Zhou L and Qi A H 2016 *Int. J. Heat Mass Trans.* **97** 631
[4] Prabhakaran M, Manikandan S, Suganthi K S, Vinodhan V L and Rajan K S 2016 *Appl. Therm. Eng.* **102** 329
[5] Crane L J 1970 *Z. Angew Math. Phys.* **21** 645
[6] Nadeem S and Lee C 2012 *Nanoscale Res. Lett.* **7** 94
[7] Nadeem S and UlHaq R *J. Aerosp. Eng.* **10** 1061
[8] Nadeem S, Mehmood R and Akbar N S 2013 *Int. J. Heat Mass Trans.* **57** 679
[9] Nadeem S, UlHaq R and Lee C 2012 *Sci. Iranica.* **19** 1550
[10] Mahapatra T R and Gupta A S 2001 *Acta Mech.* **152** 191
[11] Makinde O D 2012 *Meccanica* **47** 1173
[12] Choi S 1995 *ASME FED* **66** 99
[13] Makinde O D and Aziz A 2011 *Int. J. Therm. Sci.* **50** 1326
[14] Kuznetsov A V and Nield D A 2010 *Int. J. Therm. Sci.* **49** 243
[15] Eastman J A, Choi U S, Li S, Yu W and Thompson L J 2001 *Appl. Phys. Lett.* **78** 718
[16] Li J F and Li Z Y 2014 *Chin. Phys. B* **23** 047305
[17] Mostafa M, Hayat T, Pop I, Asghar S and Obaidat S 2011 *Int. J. Heat Mass Trans.* **54** 5588
[18] Khan W A and Pop I 2010 *Int. J. Heat Mass Trans.* **53** 2477
[19] Khan W A and Aziz A 2011 *Int. J. Therm. Sci.* **50** 1207
[20] Ibrahim W, Shankar B and Nandeppanavar M M 2013 *Int. J. Heat Mass Trans.* **56** 1
[21] Ishak A, Nazar R and Pop I 2007 *ASME J. Heat Trans.* **129** 1087
[22] Ishak A, Nazar R, Arifin R and Pop I 2007 *ASME J. Heat Trans.* **129** 1212
[23] Lok Y Y, Amin N, Campean D and Pop I 2005 *Int. J. Numer. Methods Heat Fluid Flow.* **15** 654

[24] Ishak A, Nazar R and Pop I 2008 *Comput. Math. Appl.* **56** 3188
[25] Zhang C L, Zheng L C, Zhang X X and Chen G 2015 *Appl. Math. Model.* **39** 165
[26] Lin Y H, Zheng L C, Zhang X X, Ma L X and Chen G 2015 *Int. J. Heat Mass Trans.* **84** 903
[27] Sui J Z, Zheng L C, Zhang X X and Chen G 2015 *Int. J. Heat Mass Trans.* **85** 1023
[28] Lin Y H, Zheng L C and Zhang X X 2014 *Int. J. Heat Mass Trans.* **77** 708
[29] Zheng L C, Zhang C L, Zhang X X and Zhang J H 2013 *Journal of the Franklin Institute* **350** 990
[30] Raptis A and Perdikis C 1984 *Methods Appl.* **8** 749
[31] Kumari M, Takhar H S and Nath G 1990 *Waerme-Stoffuebertrag* **25** 331
[32] Takhar H S, Kumari M and Nath G 1993 *Arch. Appl. Mech.* **63** 313
[33] Ali F M, Nazar R, Arifin N M and Pop I 2011 *Int. J. Heat Mass Trans.* **133**
[34] Ali K and Ashraf M 2012 *World Applied Sciences Journal* **16** 1615
[35] Liao S J 2003 Capman Hall/CRC Press, Boca Raton
[36] Ghotbi A R 2009 *Commun. Nonlinear Sci. Num. Simulat.* **14** 2653
[37] Liao S J 2008 *Adv. Mechan.* **15** 1
[38] Abbasbandy S 2006 *Phys. Lett. A* **360** 109
[39] Nadeem S and Saleem S 2013 *J. Taiwan Inst. Chem. Eng.* **44** 596
[40] Ahmada A, Asghar S and Alsaedi A 2015 *Chin. Phys. B* **24** 014702